Hindawi
Advances in Civil Engineering
Volume 2022, Article ID 4127660, 15 pages
https://doi.org/10.1155/2022/4127660

Research Article

Soil Deformation around a Cylindrical Cavity under Drained Conditions: Theoretical Analysis

Pieride Mabe Fogang,[1,2] **Yang Liu**,[1] **Jiale Zhao**,[1] **and Kevin Igor Azeuda Ndonfack**[1,2]

[1]*School of Civil and Resource Engineering, University of Science and Technology Beijing, Beijing 100083, China*
[2]*Department of Earth Sciences, University of Yaounde I, Yaounde, P.O. Box 812, Cameroon*

Correspondence should be addressed to Yang Liu; yangliu@ustb.edu.cn

Received 18 March 2022; Accepted 26 May 2022; Published 29 June 2022

Academic Editor: Paolo S. Valvo

This paper proposes analytical solutions to the soil deformation around a cylindrical cavity under drained conditions. Analytical procedures are used to predict the degree of interaction between cavities and ground surface loads based on mathematical theorems. The stresses applied at the boundary condition induce the ground motions around the cylindrical cavity wall. Additionally, the Airy stresses are obtained through mathematical derivatives and integrations by combining the Fourier analysis test with the Navier equations. Next, we established a schematic representation of the horizontal and vertical displacement related to the corrective shear model to obtain insight into the intensity and directions of ground stresses. The resulting transformations include displacement, shear, and deviatoric stresses applied to the cylindrical cavity wall. These data can be used as input parameters for numerical simulations to alternatively solve the groundmass redistribution problems and calibrate the horizontal stress of drained soil conditions.

1. Introduction

Many countries encourage the construction of underground structures to limit traffic and flooding on the surface. Recent technological developments allow cavities to be excavated in soft and rocky soils. These structures are usually subjected to the weight of various loads on the ground surface. Studies have shown that they cause significant deformation and displacement in tunnels. Potential ground motions are estimated on three consecutive approaches: empirical, analytical, and numerical simulation (Bao et al. [1]).

Peck [2] and Schmidt [3] proposed an empirical method on the surface settlement curve to describe the Gaussian distribution curve in equation (1). However, this method was not realistic because the measurements were performed in a single space for a half-space problem.

$$S_T\left(\tilde{x}^a, \tilde{y}^b\right) = S_0 \max \cdot e^{\left(-\left(\tilde{x}^a\right)^2/2(i)^2\right)}, \quad (1)$$

where $S_0 \max$ is the maximum settlement at the ground surface, $\tilde{x}^a = i/2\,(h/i)^{0.8}$ is the standard deviation, (i) is the diameter of the cylindrical cavity, and h is the height of the cylinder axis. Moreover, the Tresca criterion estimated the volume of soil settlement to predict soil behavior and then compared it to in-situ data (Mair and Taylor [4]). When the volume of the cylindrical cavity moves in compression at the soil surface, the volume of soil loss is estimated by $\Delta v_L = \lambda \max/i$. The soil estimation method can be adapted as a design guide for the initial displacement phase.

Moreover, the proposed analytical solutions are classified into four categories: (1) solutions based on complex variables (Verruijt [5]; Strack and Verruijt [6]; Verruijt and Booker [7]; Verruijt and Strack [8]; Wang et al. [9]; Fu et al. [10]; Fu et al. [11]; Zhang et al. [12]; Zeng et al. [13]), (2) closed-form analytical solution using the virtual image technique on the line sink (Sagaseta [14]; Verruijt and Booker [15]; Loganathan and Poulos [16]; Park [17]; Pinto and Whittle [18]), (3) the solution based on the exact prediction of the middle continues (Liu [19]; Yang et al. [20]), and (4) the general solution under the form of the airy stress function in the cartesian and polar coordinates (Bobet

[21]; Kooi and Verruijt [22]; Chou and Bobet [23]; Park [17, 24]; Pinto [25]). These analytical solutions focus on the deformation of soils at the boundary condition of underground structures and are obtained in the context of linear elasticity. Zou et al. [26] focused on employing elastoplastic theories of circular tunnels to solve geotechnical engineering problems.

Currently, several analytical solutions have been presented for the ground deformation. These solutions have also been derived assuming a conformal radial deformation model over the cavity cross section (Wang et al. [9]). Next, the ground deformation can be obtained by imposing pressure on the boundary condition concentrated toward the central axis of the cavity. The resulting analytical formula considers different stresses but is chosen with varying depths independently of the Airy stress function. Subsequently, the results of this method are generally limited to the stress distribution around the cavity. Lastly, in this paper, the analytical solution is adopted to deal with the deformation, displacement, and shear problems around the cylindrical cavity, focusing on the load-induced motions at the ground surface.

2. Definition of Problem

The geometric representation in Figure 1(a) illustrates the expansion of a cylindrical cavity under drained conditions in a two-dimensional Cartesian domain $(\widetilde{x}^a, \widetilde{y}^b)$, showing an initial state of stress with r_0 the initial radius, r the distance of the radius from the cavity axis, and $\widetilde{P}_i$ the internal pressure. Additionally, at constant static pressure, the cavity is subjected to four types of stress: horizontal stress $(\sigma_{\widetilde{x}^a})$, vertical stress $(\sigma_{\widetilde{y}^b})$, radial stress (σ_r), and tangential stress (σ_θ). According to Yu and Houlsby [27, 28], the resting soil coefficient is defined by $k_0 = 1$. As reported by Mo et al. [29], when the cavity pressure $\widetilde{p}_c$ increases slowly from its initial value, the radius of the cavity and soil (elastoplastic region) interface is expanded, respectively, (Figure 1(b)). Concerning the soil surface contact, the unique mechanical properties of the surface have a significant influence on the deformation of the soil interface (Jong et al. [30]). In the drained condition, it is assumed that although the expansion process of the cylindrical cavity is relatively slow, this may be the origin of the pore pressure related to the internal pressure $\widetilde{p}_i$ in the plastic region. Thus, the equilibrium condition in the infinite soil in cylindrical coordinates can be expressed by the following equation:

$$\frac{\partial \sigma_r}{\partial r} + \frac{\partial \varepsilon_r}{\partial r} = \frac{\sigma_\theta - \sigma_r}{r}, \tag{2}$$

where $\partial \varepsilon_r / \partial r$ is deformation Tensor. At equilibrium, equation (2) refers to two conditions, one at infinity and the second at a known value. For values of $\sigma_r(r) = -\widetilde{p}_i$ and $\sigma_r(\infty) = \widetilde{p}_\infty \approx 0$, the internal soil pressure $\widetilde{p}_i$ is considered positive when the stress fields are variable. The expansion of the cylindrical cavity and the elastic force exerted on the soil surface constitute a stress field related to the deformation, by definition of Hooke's law $\sigma(\widetilde{x}^a, \widetilde{y}^b) = \varepsilon E$ (E is Young's modulus).

3. Analytical Solution in an Infinite Elastic Soil

The equations based on the plane deformation elasticity theory are represented using the arbitrary functions imposed by the expansion problems at the boundary condition. When the expansion is accentuated at the cylindrical cavity wall, Hooke's law in all types of soils satisfies the equilibrium condition of equation (2). $\widetilde{y}^b = -(\varepsilon_{\widetilde{y}^b} / \varepsilon_{\widetilde{x}^a})$ defines the deformation induced by the vertical axial load due to static pressure. According to Muskhelishvili [31], the evaluation of deformation problems is a formula consisting of a more practical method to consider stresses and displacements as an analytical formulation. Moreover, Verruijt [5] proposes a complex variable solution to predict the elastic behavior of soils in a half-plane. These solutions are expressed in terms of two functions (ϕ and ψ) called the "Goursat function". Then, using the Cauchy-Goursat harmonic conjugation formula, the representation of the complex potential of Goursat functions becomes $\phi = \mathrm{Re}\left\{\overline{\widetilde{z}^c}\psi(\widetilde{z}^c) + \widetilde{x}^a(\widetilde{z}^c)\right\}$ (Re: real). The boundary condition is usually expressed in terms of displacement or stress. Beyond this, by integrating equation (6), the displacement related to the horizontal and vertical components imposed by the boundary condition proposed by Muskhelishvili [31] can be expressed as follows:

$$2.\mu.\left(u_{\widetilde{x}^a} + i u_{\widetilde{y}^b}\right) = (3 - 4.\nu).\phi(\widetilde{z}^c) - \widetilde{z}^c \overline{\frac{\mathrm{d}\phi}{\mathrm{d}\widetilde{z}^c}} - \overline{\psi(\widetilde{z}^c)}. \tag{3}$$

Therefore, the exact solution of the airy function is represented as follows:$F = 1/2\left\{\mathrm{Re}\left(\overline{\widetilde{z}^c}\psi(\widetilde{z}^c) + \widetilde{x}^a(\widetilde{z}^c)\right) - \overline{\psi(\widetilde{z}^c)}\right\}$.

3.1. Conformal Mapping. According to the Laplacian equation, the cartesian representation related to the complex variable methods of the potential transformed $(\widetilde{z}^c(\widetilde{x}^a, \widetilde{y}^b) \longrightarrow \zeta(\xi, \eta))$ is established by the equilibrium $\nabla^2 \phi = 0$. This potential can be rewritten in annular coordinates (Figure 2(b)) as follows:

$$\frac{\partial^2 \phi}{\partial \xi^2} + \frac{\partial^2 \phi}{\partial \eta^2} = 0. \tag{4}$$

The cavity (a) in a $\widetilde{z}^c-$ space (Figure 2(a)) is mapped to an annular region in $\zeta-$ space, on a circular ring $(\zeta = \xi + i\eta)$, of diameter 1 and inner diameter ϖ (Figure 2(b)). The conformal mapping between the intermediate geometry and the irregular geometry is written on the form (Verruijt and Booker [7]) $\widetilde{z}^c = \omega(\zeta) = -ig[(1+\zeta)/(1-\zeta)]$, $g = h(1 - \varpi^2/1 + \varpi^2)$ is a constant (h is the depth of the cylindrical cavity) and $\widetilde{y}^b = r/h$. It can be shown that $\zeta = 1$, axis $\widetilde{y}^b = 0$, with inner radius circle $|\zeta| = \varpi$, which would correspond to the boundary of the circular cylindrical cavity given by $r^2 = (\widetilde{x}^a)^2 + (\widetilde{y}^b + h)^2$. When the $\widetilde{z}^c$-space is mapped according to a circular ring in a ζ-space and bounded by the circles $|\zeta| = 1$ and $|\zeta| = \varpi$ (Figure 2), the conformal mapping can be reproduced on the form:

$$\zeta = \frac{\widetilde{z}^c\left(1 + \varpi^2\right) + ih\left(1 - \varpi^2\right)}{\widetilde{z}^c\left(1 + \varpi^2\right) - ih\left(1 - \varpi^2\right)}, \tag{5}$$

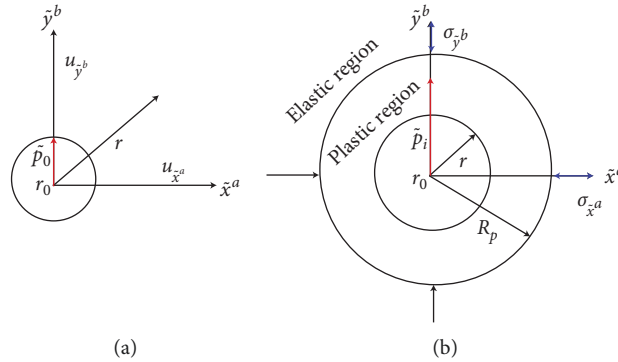

Figure 1: Schematic representation of a cylindrical cavity in infinite soil under drained conditions: (a) initial state of stress and (b) expansion of the cylindrical cavity at the stress boundary conditions.

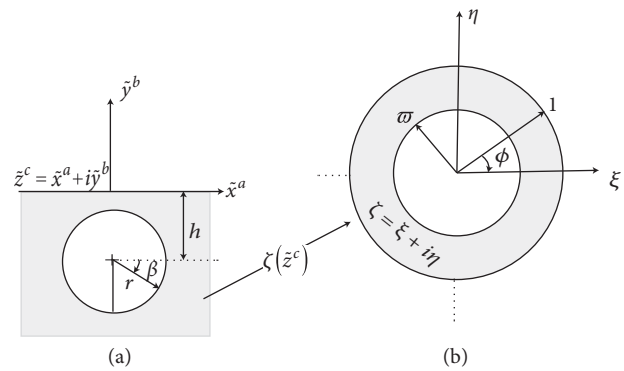

Figure 2: Conformal mapping of a cylindrical cavity represented from $\tilde{z}^c$-space to ζ-space: (a) cylindrical cavity in an infinite plane $\tilde{z}^c = \tilde{x}^a + i\tilde{y}^b$ and (b) conformal mapping $\zeta = \xi + i\eta$.

where $\varpi = (h/r - 1) + \sqrt{h/r}$. With the aid of analytic continuation and conformal mapping techniques, the complex potentials of the half-plane are expressed in a series form with some unknown coefficients, which can be determined by the Fourier expansion method (Dai et al. [32]).

Let $f(\tilde{z}^c)$ be a function admitting a single development function $f(\tilde{z}^c) = \sum_{n\in\mathbb{R}} a_n\zeta_n$. Taylor series is an excellent way to start the discussion on the Laurent series. For $n = 0$, the general formula Taylor series becomes $\sum_{n=0}^{\infty} a_0 * (\tilde{x}^a - c)^0 = a_0$. Then, by definition of the Laurent series, the two parameters of the Goursat function can be reformulated as follows:

$$\phi(\zeta) = a_0 + \sum_{n=1}^{\infty} a_n * \zeta^n + \sum_{n=1}^{\infty} b_n * \zeta^{-n}, \tag{6}$$

$$\psi(\zeta) = x_0 + \sum_{n=1}^{\infty} x_n * \zeta^n + \sum_{n=1}^{\infty} y_n * \zeta^{-n}, \tag{7}$$

where the coefficients a_n, b_n, x_n, and y_n are found by imposing the boundary condition at both boundaries (ϕ, ψ). Hence, the Laurent series parameters (x_0, x_n, and y_n) can be written as

$$x_0 = -\overline{a}_0 - \frac{1}{2}b_1 - \frac{1}{2}a_1, \tag{8}$$

$$x_n = -\overline{b}_n + (n+1)\frac{1}{2}a_{n-1} - \frac{1}{2}(n+1)a_{n+1}, \quad \text{For any } \zeta \prec n, \quad \zeta^{-n} = \overline{x}_0\zeta^{-n}, \tag{9}$$

$$y_n = -\overline{a}_n + (n+1)\frac{1}{2}b_{n-1} - \frac{1}{2}(n+1)b_{n+1}. \tag{10}$$

At the boundary condition, equation (3) can be redefined into the following equation:

$$\begin{aligned} 2\mu.u\left(\varpi.e^{i\theta}\right) = {} & 2a_0 + \frac{1}{2}\overline{b_1} + \frac{1}{2}\overline{a_1} + a_1\left(\varpi.e^{i\theta}\right) + b_1\left(\varpi.e^{i\theta}\right)^{-1} - \overline{a_1}\left(\varpi.e^{i\theta}\right) - \overline{b_1}\left(\varpi.e^{i\theta}\right)^{-1} + \cdots \\ & + b_1\left(\varpi.e^{i\theta}\right) - \overline{a_0}\left(\varpi.e^{i\theta}\right) + \overline{a_2}\left(\varpi.e^{i\theta}\right) + a_1\left(\varpi.e^{i\theta}\right) - \overline{b_0}\left(\varpi.e^{i\theta}\right) + \overline{b_2}\left(\varpi.e^{i\theta}\right). \end{aligned} \tag{11}$$

After expanding the Laurent series, the equation (11) will be expressed by following the Fourier series to the boundary condition. Similarly, Zeng et al. [33] propose a mapped function and another method to derive the mapped coefficient as an arbitrary solution in a half-plane and then as a given pressure requirement. The coefficients of equations (6) and (7) have been determined, except a_0, invariant. This coefficient remains undetermined because it is in the main chain of the Laurent series and, therefore, can be the origin of the complex variables developed by Sokolnikoff [34]. For $\zeta = 1$, the system of equations (8), (9), and (10) could be cancelled if the value were determinable. Therefore, when $k \longrightarrow \infty$ and $|\zeta| = \varpi.e^{i\theta}$, the development of the Laurent series developed in equations (3) reduces to (11), this shows that the exact analytical formula obtained is justified.

3.2. Conformal Convergence. The pre-stress radial displacement field in the cylindrical cavity can be due to the connection well around the elastic region and can be obtained by the following polar coordinate (Pinto [25]), $u_r = p_i R^2/2.\mu.r$ (R is the radius of the cylindrical cavity and pi is the hydrostatic pressure under normal convergence). Considering ordinary differential equation (ODE) under hydrostatic compression, the radial displacement can be rewritten as follows:

$$u_r = -\frac{p_i}{2.\mu}\left\{(1-2.v)r + \frac{R^2}{r}\right\}. \tag{12}$$

By simplifying equation (12), the conformal convergence parameter is set by $u_\varepsilon = -p_i R/2.\mu$; therefore, the displacement components can be expressed as follows:

$$\begin{aligned} u_{\tilde{x}^a}\left(\tilde{x}^a, \tilde{y}^b\right)|cc &= -u_\varepsilon.\frac{\tilde{x}^a R}{\left(\tilde{x}^a\right)^2 + (Y)^2}, \\ u_{\tilde{y}^b}\left(\tilde{x}^a, \tilde{y}^b\right)|cc &= -u_\varepsilon.\frac{Y.R}{\left(\tilde{x}^a\right)^2 + (Y)^2}, \end{aligned} \tag{13}$$

where cc is the conformal convergence. The horizontal and vertical components of the displacement evaluated by the radial displacement can be rewritten as follows:

$$u_{\tilde{x}^a}\left(\tilde{x}^a, \tilde{y}^b\right)|cc = u_{\varepsilon^.}\frac{1}{\tilde{x}^a R}\left(\frac{(1-2.v)\left(\left(\tilde{x}^a\right)^2 + Y^2\right)^2 + \left(\tilde{x}^a R\right)^2}{\left(\tilde{x}^a\right)^2 + Y^2}\right), \tag{14}$$

$$u_{\tilde{y}^b}\left(\tilde{x}^a, \tilde{y}^b\right)|cc = u_{\varepsilon^.}\frac{1}{Y.R}\left(\frac{(1-2.v)\left(\left(\tilde{x}^a\right)^2 + Y^2\right)^2 + (Y.R)^2}{\left(\tilde{x}^a\right)^2 + Y^2}\right). \tag{15}$$

By introducing both parameters ($Y = \tilde{y}^b + h$ and $Y = \tilde{y}^b - h$) into equations (13)–(15), the horizontal and vertical displacement components can be re-expressed as follows:

$$\begin{aligned} u_{\tilde{x}^a}\left(\tilde{x}^a, \tilde{y}^b\right)|cc &= u_\varepsilon.\frac{\tilde{x}^a.R}{\left(\tilde{x}^a\right)^2 + \left(\tilde{y}^b + h\right)^2}, \\ u_{\tilde{y}^b}\left(\tilde{x}^a, \tilde{y}^b\right)|cc &= u_\varepsilon.\frac{\left(\tilde{y}^b + h\right).R}{\left(\tilde{x}^a\right)^2 + \left(\tilde{y}^b + h\right)^2}, \end{aligned} \tag{16}$$

$$\begin{aligned} u_{\tilde{x}^a}\left(\tilde{x}^a, \tilde{y}^b\right)|cc &= u_\varepsilon.\frac{\tilde{x}^a.R}{\left(\tilde{x}^a\right)^2 + \left(\tilde{y}^b - h\right)^2}, \\ u_{\tilde{y}^b}\left(\tilde{x}^a, \tilde{y}^b\right)|cc &= u_\varepsilon.\frac{\left(\tilde{y}^b - h\right).R}{\left(\tilde{x}^a\right)^2 + \left(\tilde{y}^b - h\right)^2}, \end{aligned} \tag{17}$$

$$u_{\tilde{x}^a}\left(\tilde{x}^a, \tilde{y}^b\right)|cc = u_{\varepsilon^.}\frac{1}{R.\tilde{x}^a}\left(\frac{(1-2.v)\left(\left(\tilde{x}^a\right)^2 + \left(\tilde{y}^b + h\right)^2\right)^2 + \left(\tilde{x}^a R\right)^2}{\left(\tilde{x}^a\right)^2 + \left(\tilde{y}^b + h\right)^2}\right), \tag{18}$$

$$u_{\tilde{y}^b}\left(\tilde{x}^a,\tilde{y}^b\right)|cc = u_\varepsilon.\frac{1}{R.\left(\tilde{y}^b+h\right)}\left(\frac{(1-2.\nu)\left(\left(\tilde{x}^a\right)^2+\left(\tilde{y}^b+h\right)^2\right)^2+\left(R\left(\tilde{y}^b+h\right)\right)^2}{\left(\tilde{x}^a\right)^2+\left(\tilde{y}^b+h\right)^2}\right), \tag{19}$$

$$u_{\tilde{x}^a}\left(\tilde{x}^a,\tilde{y}^b\right)|cc = u_\varepsilon.\frac{1}{R.\tilde{x}^a}\left(\frac{(1-2.\nu)\left(\left(\tilde{x}^a\right)^2+\left(\tilde{y}^b-h\right)^2\right)^2+\left(\tilde{x}^aR\right)^2}{\left(\tilde{x}^a\right)^2+\left(\tilde{y}^b-h\right)^2}\right), \tag{20}$$

$$u_{\tilde{y}^b}\left(\tilde{x}^a,\tilde{y}^b\right)|cc = u_\varepsilon.\frac{1}{R.\left(\tilde{y}^b-h\right)}\left(\frac{(1-2.\nu)\left(\left(\tilde{x}^a\right)^2+\left(\tilde{y}^b-h\right)^2\right)^2+\left(R\left(\tilde{y}^b-h\right)\right)^2}{\left(\tilde{x}^a\right)^2+\left(\tilde{y}^b-h\right)^2}\right). \tag{21}$$

These results (equations (16) and (21)) were also proposed by Pinto [25] to evaluate the stresses applied around the cavity. The general problem of elasticity produced during conformal convergence is formulated based on vertical and horizontal stresses. This definition is based on the Navier equations, reduced according to the following stresses (equation (12)):

$$\sigma_{\tilde{x}^a}|cc = u_\varepsilon.R\left\{\begin{array}{c}\dfrac{(1-2.\nu)\left(\left(\tilde{x}^a\right)^2-\left(\tilde{y}^b-h\right)^2\right)\left[\nu.\left(\left(\tilde{y}^b-h\right)^2-\left(\tilde{x}^a\right)^2\right)+2\mu\left(\tilde{y}^b-h\right)^2\right]}{\left[R.\tilde{x}^a\left(\tilde{y}^b-h\right)\right]^2}-\ldots\\ -2\mu.\dfrac{\left(\left(\tilde{x}^a\right)^2-\left(\tilde{y}^b-h\right)^2\right)}{\left(\left(\tilde{x}^a\right)^2+\left(\tilde{y}^b-h\right)^2\right)^2}\end{array}\right\}, \tag{22}$$

$$\sigma_{\tilde{y}^b}|cc = u_\varepsilon.R\left\{\begin{array}{c}\dfrac{(1-2.\nu)\left[\left(\left(\tilde{x}^a\right)^2-\left(\tilde{y}^b-h\right)^2\right)\left(\nu.\left(\left(\tilde{y}^b-h\right)^2-\left(\tilde{x}^a\right)^2\right)-2\mu\left(\tilde{x}^a\right)^2\right)\right]}{\left[R.\tilde{x}^a\left(\tilde{y}^b-h\right)\right]^2}+\ldots\\ +2\mu.\dfrac{\left(\tilde{x}^a\right)^2\left(\left(\tilde{x}^a\right)^2-\left(\tilde{y}^b-h\right)^2\right)}{\left(\left(\tilde{x}^a\right)^2+\left(\tilde{y}^b-h\right)^2\right)^2}\end{array}\right\}. \tag{23}$$

Then, the shear stress corrected conformal displacement solutions are determined in equations (23) and (24) based on the polar parameters of the Airy function ($f_{\tilde{x}^a}=\tilde{x}^a\cos n\theta$ and $f_{\tilde{y}^b}=\tilde{y}^b\cos n\theta$), the inverse Fourier transform ($F=\sum_{n=-\infty}^{\infty}c_n\exp(-2\pi(n/t)\tilde{x}^a$, with $c_n=1/t\int_{-(t/2)}^{(t/2)}f(\tilde{x}^a)\exp[-2\pi i(n/t)]\mathrm{d}\tilde{x}^a)$, the Cauchy-Goursat biharmonic conjugation, and the elasticity theory of Boresi and Chong [35].

$$u_{\tilde{x}^a}|cc = 2u_\varepsilon R.\left(\frac{(1-\nu)\tilde{x}^a}{\left(\tilde{x}^a\right)^2+\left(\tilde{y}^b-h\right)^2}-\frac{\tilde{x}^a\left(\tilde{y}^b-h\right)\tilde{y}^b}{\left(\left(\tilde{x}^a\right)^2+\left(\tilde{y}^b-h\right)^2\right)^2}\right), \tag{24}$$

$$u_{\tilde{y}^b}|cc = u_\varepsilon R\left(\frac{\left(2\tilde{y}^b-h\left(\tilde{x}^a\right)^2-h\left(\tilde{y}^b-h\right)^2\right.}{\left(\left(\tilde{x}^a\right)^2+\left(\tilde{y}^b-h\right)^2\right)^2}-\frac{2(1-\nu)\left(\tilde{y}^b-h\right)}{\left(\tilde{x}^a\right)^2+\left(\tilde{y}^b-h\right)^2}\right). \tag{25}$$

The resulting shear stress formula is based on the equations (18) and (19) and can be rewritten as follows:

$$\tau(x,y)|cc = 2u_{\varepsilon}.\mu.R.\left\{\frac{\tilde{x}^{a}\left(2\tilde{y}^{b}-h\right)\left((1-2h)\left(\tilde{y}^{b}-h\right)^{2}-\left(\tilde{x}^{a}\right)^{2}\right)+\left(2\tilde{x}^{a}.\tilde{y}^{b}-h\right)-\ldots}{\left(\left(\tilde{x}^{a}\right)^{2}+\left(\tilde{y}^{b}-h\right)^{2}\right)^{3}}\right\}. \quad (26)$$

Deducing equations (16), (17), (23), and (24), the horizontal and vertical components of the displacement stresses compensate for each other. Summing up the equations (19), (21), and (24), the conformal vertical progress ($\Omega u_{\underset{y}{\sim}^{b}}$) around the cylindrical cavity can be defined by the following equation:

$$\Omega u_{\underset{y}{\sim}^{b}}|cc = 2.9\frac{R}{h}.u_{\varepsilon}.\ \frac{8(1-\nu)-(1-2.\nu)(R/h)^{2}}{\left((R/h)^{2}+4\right)^{2}}. \quad (27)$$

The initial solution is based on the polar radial deformation. The representative geometry in Figure 3 shows the conformal vertical progress based on the solutions resulting from the polar radial deformation. The medium properties function the different Poisson's ratios ($\nu = 0$, $\nu = 0.25$, and $\nu = 0.50$); they all converge to the value $r/h = 1$ and are constant when $r/h = 0.9$. For a constant curve variation, the load pressure at the ground surface applies a symmetrical stress distribution on the cavity boundary. Using equation (23), for $\tilde{x}^{a} = \pm h$ and $\tilde{y}^{b} = 0$, the maximum conformal horizontal motion can be expressed as follows:

$$\Gamma u_{\underset{x}{\sim}^{a}}\max|cc = \pm u_{\varepsilon}(1-\nu)\frac{R}{h}. \quad (28)$$

Hence, the conformal vertical motion (equation (24)) $\tilde{y}^{b} = 0$ and $\tilde{x}^{a} = \pm h$, the maximum conformal vertical motion can be obtained as follows:

$$\Gamma u_{\underset{y}{\sim}^{b}}\max|cc = \pm\frac{R}{h(u\varepsilon)}(1-\nu)-\frac{1}{2}. \quad (29)$$

Equations (27) and (28) can be considered the maximum displacement induced by the loads at the ground surface. When $\Gamma u_{\underset{x}{\sim}^{a}}|cc = \Gamma u_{\underset{y}{\sim}^{b}}|cc = 0$, with $\tilde{z}^{c} = 0$; therefore $\overline{\mathrm{d}\phi/\mathrm{d}\tilde{z}^{c}} = 0$. The maximum motions in the boundary condition can be due to the elastic stress forces exerted by the principal axes $(\sigma_r, \sigma_\theta)$ on the initial radius r_0. In this vein, the hypothesis of Verruijt (5) seems to be the most appropriate in this paper because, after excavation, the load-induced conditions on the ground surface apply forces that can be damped either by the cavity wall or by the thickness of the lining. The geometry in Figure 4 was realized by adding equations (21)–(24), (31), and (32). It shows the displacements on each half-plane of the cavity performing convergent motions toward the initial radius. Beyond this, symmetry is observed on each half-plane of the cavity, resulting in a nonuniform convergence when the vertical load is greater than the horizontal load. The ground displacement is not a function of ν and R/h, but $\tilde{x}^{a}/h$ and $\tilde{y}^{b}/h$ coordinates.

3.3. Near and Far Field Non-Uniform Deformation. The components of the initial state displacement of the cylindrical cavity are defined by the elastic constitutive relation as presented by Pinto [25], defining the following relations:

$$u_{\underset{\tilde{x}}{\sim}^{a}}|nd = \frac{q_i}{2.\mu}\tilde{x}^{a};\ u_{\underset{y}{\sim}^{b}}|nd = -\frac{q_i}{2.\mu}\tilde{y}^{b}, \quad (30)$$

where *nd* is the nonuniform deformation and *qi* is the hydrostatic pressure under nonuniform deformation.. At the boundary condition, the pure distortion parameter of a cylindrical cavity (u_δ) is defined by Pinto [25], $u_\delta = (3-4.\nu)(q_i.R/2.\mu)$. In cylindrical coordinates, a specific biharmonic function can be used as the Airy stress function according to the formula $F_{(\underset{\tilde{x}}{\sim}^{a},\underset{y}{\sim}^{b})} = d_n(r^{-n+2}\cos n\theta)$. Additionally, some analyses by Hua and Dai [36] based on the consistency of the concentration obtained by the analytical algorithm on the real solution are joined with the approximate explicit solution to evaluate the cylindrical cavity when the depth increases. However, the stress concentration around the hole is proposed by a complex potential on a half-plane, representing in a specific form unknown coefficients, determined by prescribed boundary conditions (Dai et al., [37]). Using the compatibility equation, the biharmonic function that can be used as the Airy stress function can be defined as follows:

$$F_{(r)}|nd = \left(X.r^{n+2}+Y.r^{n}+Z.r^{-n+2}+T.r^{-n}\right)\cos n\theta, \quad (31)$$

where X, Y, Z, and T are constants. The elastoplastic solution as a function of stresses σ_r, σ_θ, and $\tau_{(r,\theta)}$ (in the far-field, $\sigma_{r(r\longrightarrow\infty)}|nd = 0$, $\sigma_{\theta(r\longrightarrow\infty)}|nd = 0$ and angle θ is negligible) will yield stress tensors related to equation (38). On this subject, as presented by Aghchai et al. [38], the airy stress function formulation is based on the general idea of developing a representation for the stress field that satisfies the equilibrium and gives a single governing equation from the

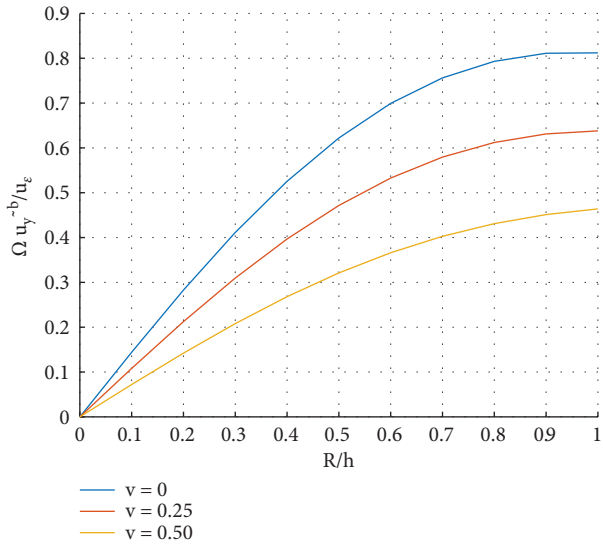

Figure 3: Vertical progress based on conformal convergence.

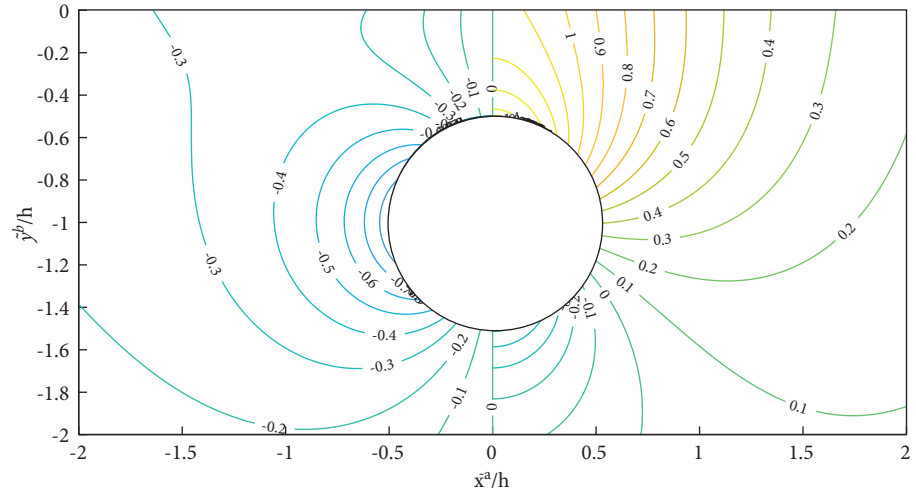

Figure 4: Stratigraphic deformation due to conformal contraction (u_ε/u_δ).

compatibility statement. By integrating into the theory of elasticity proposed by Boresi and Chong [35], the derivatives of the components of the Airy stress and the biharmonic conjugate of Cauchy-Goursat, the displacement in non-uniform deformation (Figure 5) becomes

$$u_{i\tilde{x}^a}\left(\tilde{x}^a,\tilde{y}^b\right)|nd = u_\delta \frac{R}{(3-4\gamma)}.\tilde{x}^a.\ \frac{\left(\left(\tilde{x}^a\right)^2+Y^2\right).\left[4\left(\begin{array}{c}(1-\nu).\\ \left(\left(\tilde{x}^a\right)^2+Y^2\right)-Y\end{array}\right)\right]-R^2.\left(\left(\tilde{x}^a\right)^2-3Y^2\right)}{\left(\left(\tilde{x}^a\right)^2+Y^2\right)^3}, \tag{32}$$

$$u_{i\tilde{y}^b}\left(\tilde{x}^a,\tilde{y}^b\right)|nd = -u_\delta \frac{R}{(3-4\gamma)}.Y.\ \frac{\left(\left(\tilde{x}^a\right)^2+Y^2\right).\left[\left(\begin{array}{c}4(1-\nu).\\ \left(\left(\tilde{x}^a\right)^2+Y^2\right)-\tilde{x}^a\end{array}\right)\right]+R^2.\left(3\left(\tilde{x}^a\right)^2-Y^2\right)}{\left(\left(\tilde{x}^a\right)^2+Y^2\right)^3}. \tag{33}$$

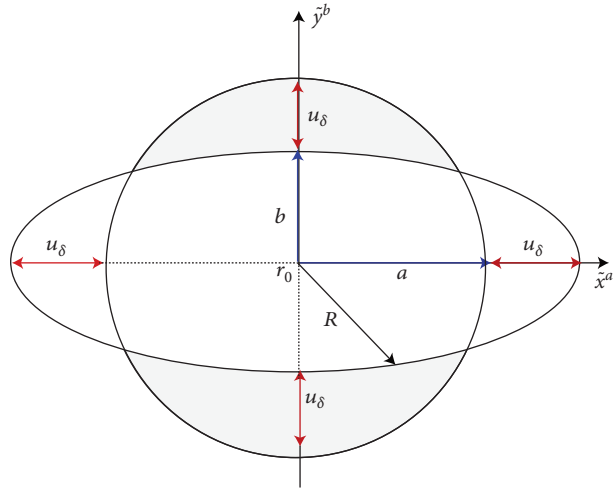

FIGURE 5: Nonuniform deformation (a and b are the dimensions of the ellipsoid).

Equations (31), (32), and Pinto [25] show a significant difference in the biharmonic function derived from equation (30). Considering $1/R^2.(r)^3 \approx 0$, the displacement components in the far-field can be established as follows:

$$u_{\tilde{x}^a}\left(\tilde{x}^a, \tilde{y}^b\right)|nd = u_\delta \frac{4(1-\nu)}{(3-4.\nu)}.R.\tilde{x}^a.\frac{\left(\left(\tilde{x}^a\right)^2 + Y^2\right) - (Y/(1-\nu))}{\left(\left(\tilde{x}^a\right)^2 + Y^2\right)^2}, \tag{34}$$

$$u_{\tilde{y}^b}\left(\tilde{x}^a, \tilde{y}^b\right)|nd = -u_\delta \frac{4(1-\nu)}{(3-4.\nu)}.R.Y.\ \frac{\left(\left(\tilde{x}^a\right)^2 + Y^2\right) - \tilde{x}^a/(1-\nu)}{\left(\left(\tilde{x}^a\right)^2 + Y^2\right)^2}. \tag{35}$$

The displacement (equations (31) and (32)) can be re-established as follows $Y = \tilde{y}^b + h$:

$$\begin{pmatrix} \left(\tilde{x}^a\right)^2 + \\ \left(\tilde{y}^b + h\right)^2 \end{pmatrix}.\left[4\left((1-\nu).\begin{pmatrix} \left(\tilde{x}^a\right)^2 + \\ \left(\tilde{y}^b + h\right)^2 \end{pmatrix} - \left(\tilde{y}^b + h\right)\right)\right] - \cdots$$

$$u_{i\left(\tilde{x}^a\right)}\left(\tilde{x}^a, \tilde{y}^b\right)|nd = u_\delta \frac{R}{(3-4.\nu)}.\tilde{x}^a.\ \frac{-R^2\left(\left(\tilde{x}^a\right)^2 - 3\left(\tilde{y}^b + h\right)^2\right)}{\left(\left(\tilde{x}^a\right)^2 + \left(\tilde{y}^b + h\right)^2\right)^3}, \tag{36}$$

$$\left(\left(\tilde{x}^a\right)^2 + \left(\tilde{y}^b + h\right)^2\right).\left[\left(4(1-\nu).\begin{pmatrix} \left(\tilde{x}^a\right)^2 + \\ \left(\tilde{y}^b + h\right)^2 \end{pmatrix} - x\right)\right] + \cdots$$

$$u_{i\left(\tilde{y}^b\right)}\left(\tilde{x}^a, \tilde{y}^b\right)|nd = -u_\delta \frac{R}{(3-4.\nu)}.\left(\tilde{y}^b + h\right)\ \frac{+R^2\left(3\left(\tilde{x}^a\right)^2 - \left(\tilde{y}^b + h\right)^2\right)}{\left(\left(\tilde{x}^a\right)^2 + \left(\tilde{y}^b + h\right)^2\right)^3}. \tag{37}$$

Equations (31) and (32) can be given as $Y = \tilde{y}^b - h$:

$$\left((\tilde{x}^a)^2 + \left(\tilde{y}^b - h\right)^2\right)\left[4\left((1-\nu)\begin{pmatrix}(\tilde{x}^a)^2 + \\ \left(\tilde{y}^b - h\right)^2\end{pmatrix} - \left(\tilde{y}^b - h\right)\right)\right] - \cdots$$

$$u_{ii\,(\tilde{x}^a)}\left(\tilde{x}^a, \tilde{y}^b\right)|nd = u_\delta \frac{R}{(3-4.\nu)}.\tilde{x}^a.\ \frac{-R^2\left((\tilde{x}^a)^2 - 3\left(\tilde{y}^b - h\right)^2\right)}{\left((\tilde{x}^a)^2 + \left(\tilde{y}^b - h\right)^2\right)^3}, \tag{38}$$

$$\left((\tilde{x}^a)^2 + \left(\tilde{y}^b - h\right)^2\right)\left[\left(4(1-\nu)\begin{pmatrix}(\tilde{x}^a)^2 + \\ \left(\tilde{y}^b - h\right)^2\end{pmatrix} - \tilde{x}^a\right)\right] + \cdots$$

$$u_{ii\,(\tilde{y}^b)}\left(\tilde{x}^a, \tilde{y}^b\right)|nd = -u_\delta \frac{R}{(3-4.\nu)}.\left(\tilde{y}^b - h\right).\ \frac{+R^2\left(3(\tilde{x}^a)^2 - \left(\tilde{y}^b - h\right)^2\right)}{\left((\tilde{x}^a)^2 + \left(\tilde{y}^b - h\right)^2\right)^3}. \tag{39}$$

Then, equations (33) and (34) becomes (far-field displacement):

$$u_{\tilde{x}^a}\left(\tilde{x}^a, \tilde{y}^b\right)|nd = u_\delta \frac{4(1-\nu)}{(3-4.\nu)}.R.\tilde{x}^a.\ \frac{\left((\tilde{x}^a)^2 + \left(\tilde{y}^b + h\right)^2\right) - (1/(1-\nu)).\left(\tilde{y}^b + h\right)}{\left((\tilde{x}^a)^2 + \left(\tilde{y}^b + h\right)^2\right)^2}, \tag{40}$$

$$u_{\tilde{y}^b}\left(\tilde{x}^a, \tilde{y}^b\right)|nd = -u_\delta \frac{4(1-\nu)}{(3-4.\nu)}.R.\left(\tilde{y}^b + h\right).\ \frac{\left((\tilde{x}^a)^2 + \left(\tilde{y}^b + h\right)^2\right) - (1/1-\nu).\tilde{x}^a}{\left((\tilde{x}^a)^2 + \left(\tilde{y}^b + h\right)^2\right)^2}. \tag{41}$$

Equations (31) and (34) can be established as follows:

$$u_{\tilde{x}^a}\left(\tilde{x}^a, \tilde{y}^b\right)|nd = u_\delta \frac{4(1-\nu)}{(3-4.\nu)}.R.\tilde{x}^a.\ \frac{\left((\tilde{x}^a)^2 + \left(\tilde{y}^b - h\right)^2\right) - (1/(1-\nu)).\left(\tilde{y}^b - h\right)}{\left((\tilde{x}^a)^2 + \left(\tilde{y}^b - h\right)^2\right)^2}, \tag{42}$$

$$u_{\tilde{y}^b}\left(\tilde{x}^a, \tilde{y}^b\right)|nd = -u_\delta \frac{4(1-\nu)}{(3-4.\nu)}.R.\left(\tilde{y}^b - h\right).\ \frac{\left((\tilde{x}^a)^2 + \left(\tilde{y}^b - h\right)^2\right) - (1/(1-\nu)).\tilde{x}^a}{\left((\tilde{x}^a)^2 + \left(\tilde{y}^b - h\right)^2\right)^2}. \tag{43}$$

The approximate shear stress in the far-field is determined by the equations (39)–(42).

The discontinuity lines shown in Figure 6 all converge on the central and median axis of the cylindrical cavity. This means that the horizontal and vertical displacement can be mathematically established by $u_{\tilde{x}^a} = \tilde{x}^a/h.u_{\tilde{y}^b}$. For $r/h = 0.25$ (Figure 7), the horizontal and vertical motion curves for different values of the Poisson's ratio all converge to $u_{\tilde{x}^a}/u_\delta = 0$ and $u_{\tilde{y}^a}/u_\delta = 0$. On this subject, the Sagaseta [14] theorem on both sides of the mirror is respected in the far-field of the cylindrical cavity. Hence, a series solution for the stress distribution in the half-plane is derived using conformal mapping techniques and Fourier expansions (Dai et al. [39]). In this case, by evaluating the displacement

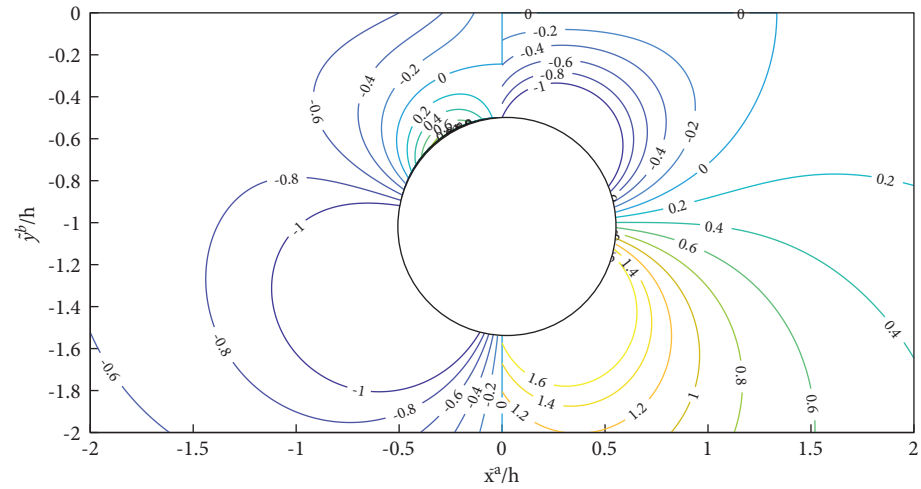

Figure 6: Displacement of the far-field ($u_{\tilde{x}^a}/u_\delta$, $u_{\tilde{y}^b}/u_\delta$).

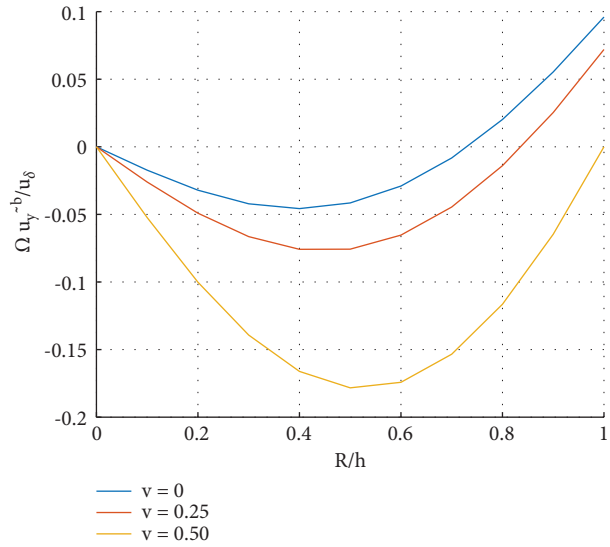

Figure 7: Vertical progress induced by nonuniform deformation.

induced by the vertical stress ($R^2 \approx h^2$) and including the inverse Fourier transform $F_{(n)} = i/2\pi \int_{\omega=2\pi i} \tau_{(\omega)} \exp(-i\omega n\Delta t)\mathrm{d}\omega$, the nonuniform displacement rectified by the shear stress on the near-field can be established as follows:

$$u_{iii\,(\tilde{x}^a)}\left(\tilde{x}^a, \tilde{y}^b\right)|nd = \frac{3u_\delta R}{3-4.\nu}\left[\begin{array}{c} \dfrac{\left[(1-\nu)\left(\tilde{x}^a.\left(\left(\tilde{x}^a\right)^2+\left(\tilde{y}^b\right)^2-h^2\right)\right)\right]}{\left(\left(\tilde{x}^a\right)^2+\left(\tilde{y}^b-h\right)^2\right)^3}-\ldots \\ -\left(\left(\tilde{x}^a\right)^2+\left(\tilde{y}^b-h\right)^2\right)\left(\begin{array}{c}\tilde{y}^b\left(\tilde{y}^b-h\right).h+2h\left(\tilde{x}^a\right)^2 \\ -\left(\tilde{y}^b-th\right)\end{array}\right)+\ldots \\ \dfrac{+3\left(\left(\tilde{x}^a\right)^2.h-\left(\tilde{y}^b-h\right)\right)\left(\left(\tilde{y}^b-h\right)^2+h\left(\tilde{y}^b-h\right)+\left(\tilde{x}^a\right)^2\right)}{\left(\left(\tilde{x}^a\right)^2+\left(\tilde{y}^b-h\right)^2\right)^4} \end{array}\right], \tag{44}$$

$$u_{iii(\widetilde{y}^b)}\left(\widetilde{x}^a,\widetilde{y}^b\right)=\frac{3u_\delta R}{3-4\nu}.\left[\begin{array}{l}\dfrac{\left[(1-\nu)\left((\widetilde{x}^a)^2\left(2h-\widetilde{y}^b\right)-\widetilde{y}^b\left(\widetilde{y}^b-h\right)^2\right)\right]}{\left((\widetilde{x}^a)^2+\left(\widetilde{y}^b-h\right)^2\right)^3}+\\ \left((\widetilde{x}^a)^2+\left(\widetilde{y}^b-h\right)^2\right).\left[\begin{array}{c}\left(\widetilde{y}^b-h\right)^2+\\ h\left(\left(\widetilde{y}^b-h\right)+(\widetilde{x}^a)^2-(\widetilde{x}^a)^2\left(2\widetilde{y}^b-h\right)h\right)\\ +\left(\widetilde{y}^b-h\right)\left(2\widetilde{y}^b-h\right)\end{array}\right]+\ldots\\ +\dfrac{6\left(\widetilde{y}^b-h\right)\left\{\left(h.(\widetilde{x}^a)^2-\left(\widetilde{y}^b-h\right)\right)\left(\left(\widetilde{y}^b-h\right)^2+h\left(\widetilde{y}^b-h\right)+(\widetilde{x}^a)^2\right)\right\}}{\left((\widetilde{x}^a)^2+\left(\widetilde{y}^b-h\right)^2\right)^4}\end{array}\right]. \tag{45}$$

In this vein, the displacement components induced by the nonuniform deformation are derived from the superposition of the displacement components (equations (35)–(38)) and the equilibrium displacement field after excavation (Figure 8; $U_{(\widetilde{x}^a)}|nd=u_{i(\widetilde{x}^a)}|nd+u_{ii(\widetilde{x}^a)}|nd+u_{iii(\widetilde{x}^a)}|nd$ and $U_{(\widetilde{y}^b)}|nd=u_{i(\widetilde{y}^b)}|nd+u_{ii(\widetilde{y}^b)}|nd+u_{iii(\widetilde{y}^b)}|nd$). Thus, in the region $-h\prec\widetilde{x}^a\prec h$, the vertical displacement is larger than the horizontal displacement. This convergence is also noticeable in Figure 9. The vertical progress imposed on the nonuniform deformation ($\Omega u_{\underset{\sim}{y}^b}$) can be established by the following equation:

$$\Omega u_{\underset{\sim}{y}^b}\left(\widetilde{x}^a,\widetilde{y}^b\right)|nd=\frac{2}{(3-4.\nu)}.u_\delta.\ \frac{R}{h}\left\{\frac{(7-4.\nu)(R/h)^4+4(7-8.\nu)(R/h)^2-17}{\left((R/h)^2+4\right)^3}\right\}. \tag{46}$$

The geometric representation in Figure 7 shows a concavity downwards (with $R/h > 1.1$ and $\nu = 0.5$). Thus, the load-induced ground deformation at the ground surface applies compressive pressure to the cylindrical cavity wall ($R \approx h$). For a shallow cylindrical cavity, the probability of vertical displacement is much higher than in deep cavities. Therefore, the variations of the complex solutions presented by Verruijt and Booker [15] demonstrate the assertion of the exact solution presented in equation (3).

By adding the two displacement parameters given by the approximate solution (equation (37)), $\widetilde{y}^b = 0$, with $\widetilde{x}^a = \pm h$, the maximum horizontal motion in nonuniform deformation can be expressed as

$$\Gamma u_{\underset{\sim}{x}^a}\max|nd=\pm\frac{u_\delta}{(3-4.\nu)}\ \frac{R}{h}\left\{(2(1-\nu)+h)+\frac{1}{4}\left(\frac{R}{h}\right)^2\right\}. \tag{47}$$

Hence, the maximum vertical motion in nonuniform deformation can be reduced to the following formula (equation 38; with $\widetilde{y}^b = 0$):

$$\Gamma u_{\underset{\sim}{y}^b}\max|nd=\pm\frac{u_\delta}{(3-4.\nu)}\ \frac{R}{h}.\left[\frac{\left(7-8.\nu+4(R/h)^3\right)}{3}\right]. \tag{48}$$

For $\widetilde{y}^b = \pm h$, the maximum vertical motion can be reduced to zero. Thus, for different values of $\nu = 0.00$, $\nu = 0.25$, and $\nu = 0.50$, with $R = h$ for shallow cavities, is equal to $\Gamma u_{\underset{\sim}{y}^b}\max|nd=\pm 1.2u_\delta$, $\Gamma u_{\underset{\sim}{y}^b}\max|nd=\pm 1.5u_\delta$, and $\Gamma u_{\underset{\sim}{y}^b}\max|nd=\pm 2.3u_\delta$. Analytical solutions are precious for the conceptual understanding of the mechanical behavior of noncircular cavities and the validation of numerical models (Wang et al. [40]). It is important to note that soil settlement is related to the pressure at the soil surface. Next, the stress distribution around the cavity can induce conformal convergence, nonuniform deformation, and vertical progression (Figure 10).

4. Discussion

The geometric representation in Figure 11 is the superposition of the conformal vertical displacement and the vertical progress of the tunnel spring line for the approximate solution of the uniform convergence mode (Pinto [25]). Next, the two solutions show similarities in the values of the Poisson's ratio ($\nu = 0$, $\nu = 0.25$, and $\nu = 0.50$), and the orthogonal projection of the curves, which all converge to the value $r/h = 1$. The comparison shows that the conformal vertical progression resulting from equation (26) is two times smaller than the value proposed by Pinto and Whittle [41].

This difference is due to the partial derivatives and mathematical integration resulting from the Fourier analysis test and Navier's equations on the radial displacement during hydrostatic compression. Such a solution may be more suitable for shallow tunnels as it can also predict settlement movements when the tunnel has a variable internal pressure.

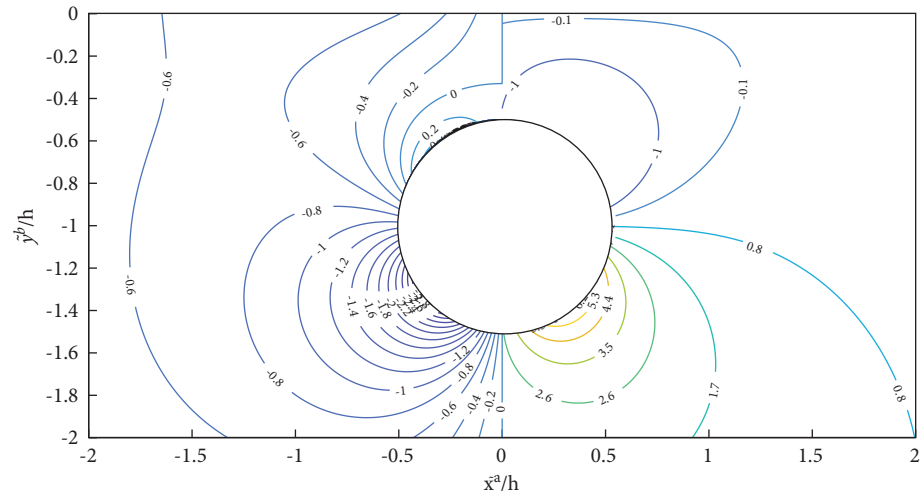

Figure 8: Ground displacement for nonuniform deformation ($u_{\bar{x}}^{\bar{a}}/u_\delta$and $u_{\bar{y}}^{\bar{b}}/u_\delta$).

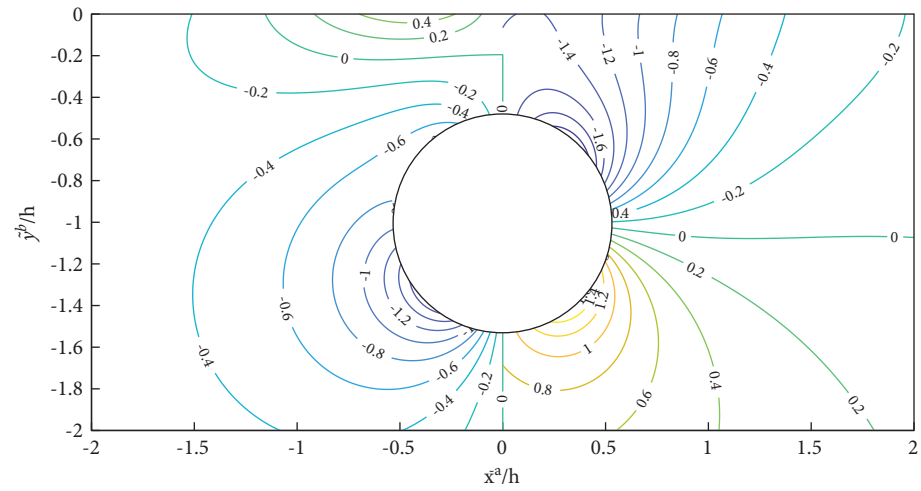

Figure 9: Deformation due to the conformal contraction (u_ϵ/u_δ).

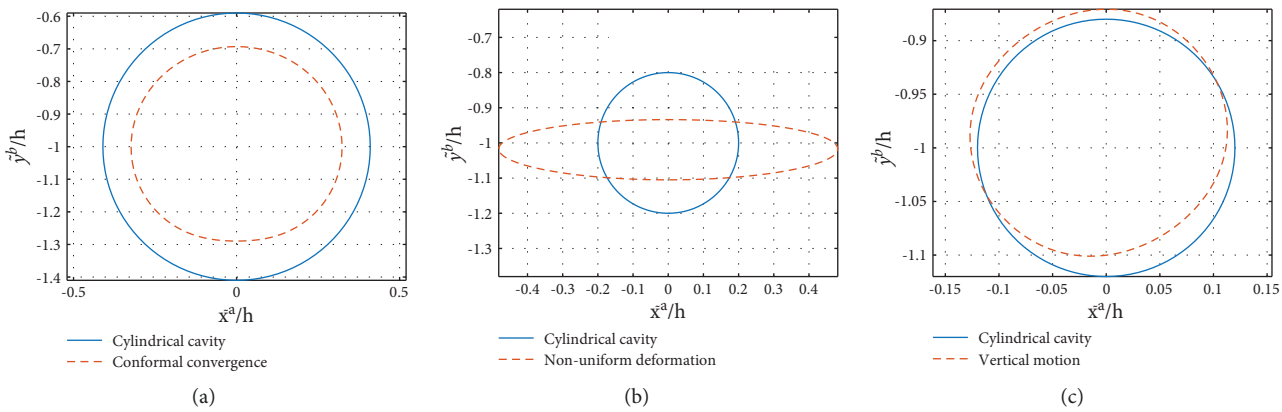

Figure 10: Displacement of the cylindrical cavity: (a) conformal convergence, (b) nonuniform deformation, and (c) vertical motion.

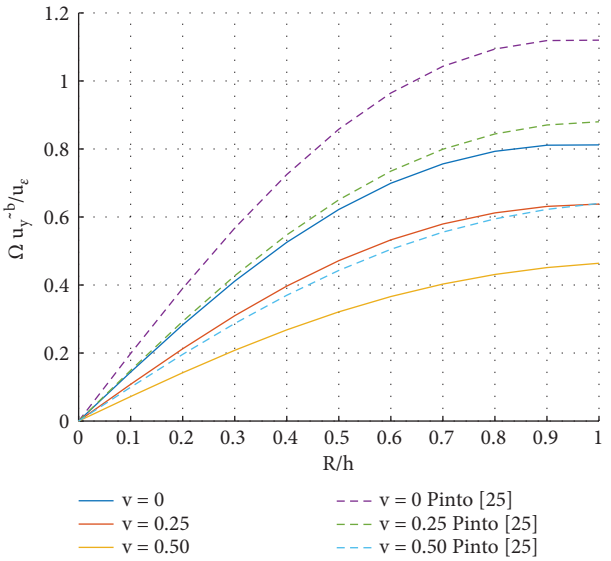

Figure 11: Relationship between the conformal vertical progress and the vertical translation of tunnel spring line.

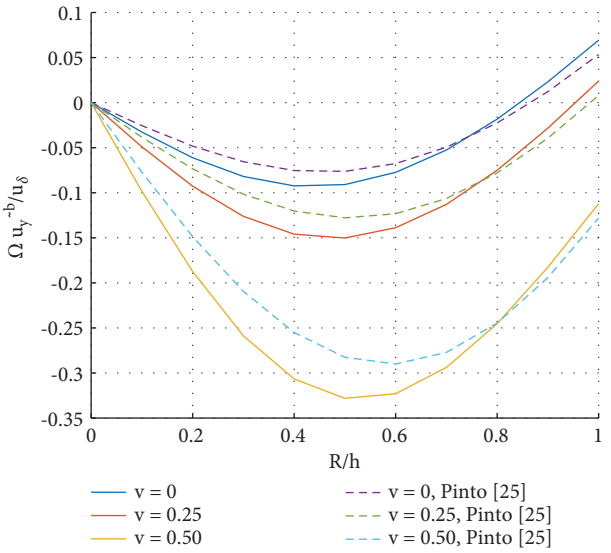

Figure 12: Relationship between vertical progress with nonuniform deformation and vertical translation of the spring line.

In this study, Figure 12 shows the relationship between the vertical progress imposed by the nonuniform deformation on the cavity wall and the vertical translation of the spring line proposed by Pinto [25]. These solutions all exhibit concavity at $r/h = 0.5$, and all converge at the $r/h = 1$ point. It is therefore essential to note that the provided solutions give satisfactory results.

5. Conclusion

This paper presents analytical solutions to soil deformation around a cylindrical cavity under drained conditions. Analytical methods based on mathematical formulas were proposed considering three deformation parameters: conformal convergence, nonuniform deformation, and horizontal and vertical ground motion. The integration of the ground deformation methods was based on approximate solutions referring to the exact solutions. Additionally, other predictive models of soil behavior resulting mainly from the geometry and stability index were suggested to compensate for the redistribution of stresses at the wall of the cylindrical cavity.

(1) The model related to the conformal convergence (u_ε) was defined on the approach of continuous numerical functions in a 2D Cartesian plane, introduced by the radial displacement pre-stress applied to the boundary condition. The stresses were redistributed uniformly at the cavity wall, inducing the displacement determined by the Airy stress. Thus, the expansion rate influenced by the excavation speed impacting the initial soil stresses was determined by the maximum soil movements ($\Gamma u_{\tilde{x}}^{a}$ max and $\Gamma u_{\tilde{y}}^{b}$ max) and was established for varying Poisson's ratios ($0 \prec v \prec 1$) values.

(2) The nonuniform deformation (u_δ) based on the biharmonic function was defined on the initial stress state of the soil, according to the elastic constitutive relation. The near and far-fields were evaluated using the asymmetric stress distribution around the excavation trough. Furthermore, a settlement model induced by the deformed soil was related to the pressure at the soil surface due to the void created by the excavation. Then, the corrective shear pressure was obtained by the maximum components. The shear pressure and its relatively high traction balance the forces that could lead to its deformation. Thus, when the load applied to the ground surface is less, the minimum components assumption cannot be applied because the traction pressure could induce a rebound leading to the buoyancy of the cylindrical cavity.

(3) Finally, a comparison of the results with previous work has shown that the analytical solution of a cylindrical cavity could predict the ground motion either by the rate of ground excavation modifying the initial conditions of the environment or by the variations of load on the ground surface.

Data Availability

All data, models, and code generated or used during the study are available from the corresponding author upon reasonable request.

Conflicts of Interest

The authors declare that they have no conflicts of interest.

Acknowledgments

The authors would like to acknowledge the National Key R&D Program of China (2017YFC0805300), who funded this project.

References

[1] Z. Bao, Y. Yuan, and H. Yu, "Multi-scale physical model of shield tunnels applied in shaking table test," *Soil Dynamics and Earthquake Engineering*, vol. 100, pp. 465–479, 2017.

[2] R. B. Peck, "Deep excavations and tunneling in soft ground," in *Proceedings of the 7th International Conference on Soil Mechanics and Foundation Engineering*, pp. 225–290, State of the Art, Netherlands, Europe, 1969.

[3] B. Schmidt, *Settlements and Ground Movements Associated with Tunnelling in Soils*, Ph.D. thesis, University of Illinois, Illinois, IL, Champaign, 1969.

[4] R. J. Mair and R. N. Taylor, "Prediction of clay behavior around tunnels using plasticity solutions Predictive Soil Mechanics," in *Proceedings of the Wroth Memorial Symposium*, pp. 27–29, Thomas Telford Limited, London, UK, July 1992.

[5] A. Verruijt, "A complex variable solution for a deforming circular tunnel in an elastic half-plane," *International Journal for Numerical and Analytical Methods in Geomechanics*, vol. 21, no. 2, pp. 77–89, 1997.

[6] O. E. Strack and A. Verruijt, "A complex variable solution for the ovalization of a circular tunnel in an elastic half-plane," in *Proceedings of the Geo Engineering, an International Conference on Geotechnical and Geological Engineering*, Technomics, Melbourne, VIC, Australia, November 2000.

[7] A. Verruijt and J. R. Booker, "Complex variable analysis of Mindlin's tunnel problem." proceedings of the Booker Memorial Symposium," *Developments in Theoretical Geomechanics*, pp. 3–22, Balkema, Netherlands, Europe, 2000.

[8] A. Verruijt and O. E. Strack, "Buoyancy of tunnels in soft soils," *Géotechnique*, vol. 58, no. 6, pp. 513–515, 2008.

[9] L.-Z. Wang, L.-L. Li, and X.-J. Lv, "Complex variable solutions for tunneling-induced ground movement," *International Journal of Geomechanics*, vol. 9, no. 2, pp. 63–72, 2009.

[10] J. Y. Fu, J. S. Yang, L. Yan, and S. M. Abbas, "An analytical solution for deforming twin-parallel tunnels in an elastic half-plane," *International Journal for Numerical and Analytical Methods in Geomechanics*, vol. 39, no. 5, pp. 524–538, 2015.

[11] J. Fu, J. Yang, H. Klapperich, and S. Wang, "Analytical prediction of ground movements due to a nonuniform deforming tunnel," *International Journal of Geomechanics*, vol. 16, no. 4, Article ID 04015089, 2016.

[12] Z. Zhang, M. Huang, C. Zhang, K. Jiang, Z. Wang, and X. Xi, "Complex variable solution for twin tunneling-induced ground movements considering nonuniform convergence pattern," *International Journal of Geomechanics*, vol. 20, no. 6, Article ID 04020060, 2020.

[13] G. Zeng, H. Wang, and M. Jiang, "Analytical study of ground responses induced by the excavation of quasirectangular tunnels at shallow depths," *International Journal for Numerical and Analytical Methods in Geomechanics*, vol. 43, no. 13, pp. 2200–2223, 2019.

[14] C. Sagaseta, "Analysis of undrained soil deformation due to ground loss," *Géotechnique*, vol. 37, no. 3, pp. 301–320, 1987.

[15] A. Verruijt and J. R. Booker, "Surface settlements due to deformation of a tunnel in an elastic half-plane," *Géotechnique*, vol. 46, no. 4, pp. 753–756, 1996.

[16] N. Loganathan and H. G. Poulos, "Analytical prediction for tunneling-induced ground movements in clays," *Journal of Geotechnical and Geoenvironmental Engineering*, vol. 124, no. 9, pp. 846–856, 1998.

[17] K. H. Park, "Elastic solution for tunneling-induced ground movements in clays," *International Journal of Geomechanics*, vol. 4, no. 4, pp. 310–318, 2004.

[18] F. Pinto and A. J. Whittle, "Ground movements due to shallow tunnels in soft ground. I analytical solutions," *Journal of Geotechnical and Geoenvironmental Engineering*, vol. 140, no. 4, Article ID 04013040, 2014.

[19] B. Liu, "Theory of stochastic medium and its application in surface subsidence due to excavation," *Transactions of Nonferrous Metals Society of China*, vol. 2, no. 3, pp. 17–24, 1992.

[20] J. S. Yang, B. C. Liu, and M. C. Wang, "Modeling of tunneling induced ground surface movements using stochastic medium theory," *Tunnelling and Underground Space Technology*, vol. 19, no. 2, pp. 113–123, 2004.

[21] A. Bobet, "Analytical solutions for shallow tunnels in saturated ground," *Journal of Engineering Mechanics*, vol. 127, no. 12, pp. 1258–1266, 2001.

[22] C. B. Kooi and A. Verruijt, "Interaction of circular holes in an infinite elastic medium," *Tunnelling and Underground Space Technology*, vol. 16, no. 1, pp. 59–62, 2001.

[23] W. I. Chou and A. Bobet, "Predictions of ground deformations in shallow tunnels in clay," *Tunnelling and Underground Space Technology*, vol. 17, no. 1, pp. 3–19, 2002.

[24] K. H. Park, "Analytical solution for tunnelling-induced ground movement in clays," *Tunnelling and Underground Space Technology*, vol. 20, no. 3, pp. 249–261, 2005.

[25] F. Pinto, "Analytical Methods to Interpret Ground Deformations Due to Soft Ground Tunneling," S M thesis, Dept. of Civil and Environmental Engineering, Massachusetts Institute of Technology (MIT), Cambridge, England, 1999.

[26] J. F. Zou, K. F. Chen, and Q. J. Pan, "An improved numerical approach in surrounding rock incorporating rockbolt effectiveness and seepage force," *Acta Geotechnica*, vol. 13, no. 3, pp. 707–727, 2018.

[27] H. S. Yu and G. T. Houlsby, "Finite cavity expansion in dilatant soils: loading analysis," *Géotechnique*, vol. 41, no. 2, pp. 173–183, 1991.

[28] H. S. Yu and G. T. Houlsby, "A large strain analytical solution for cavity contraction in dilatant soils," *International Journal for Numerical and Analytical Methods in Geomechanics*, vol. 19, no. 11, pp. 793–811, 1995.

[29] P. Q. Mo, A. M. Marshall, and H. S. Yu, "Elastic-plastic solutions for expanding cavities embedded in two different cohesive-frictional materials," *International Journal for Numerical and Analytical Methods in Geomechanics*, vol. 38, no. 9, pp. 961–977, 2014.

[30] Y.-G. Jong, Y. Liu, Z. Chen, and P. Mabe Fogang, "Hypoplastic interface model considering plane strain condition and surface roughness," *Advances in Civil Engineering*, vol. 2021, Article ID 1473181, 13 pages, 2021.

[31] Muskhelishvili, *Some Basic Problems of the Mathematical Theory of Elasticity*P. Noordhoff Ltd, Netherlands, Europe, 1963.

[32] M. Dai, C.-F. Gao, and C. Q. Ru, "Surface tension-induced stress concentration around a nanosized hole of arbitrary shape in an elastic half-plane," *Meccanica*, vol. 49, no. 12, pp. 2847–2859, 2014.

[33] G. Zeng, H. Cai, and A. Lu, "An Analytical Solution for an Arbitrary Cavity in an Elastic Half-Plane," *Rock Mechanics and Rock Engineering*, vol. 52, 2019.

[34] I. S. Sokolnikoff, *Mathematical Theory of Elasticity*, McGraw-Hill, New York, NY, USA, 1956.

[35] A. P. Boresi and K. P. Chong, *"Elasticity in Engineering Mechanics"*, pp. 394–397, Elsevier Science, Netherlands, Europe, 1987.

[36] J. Hua and M. Dai, "Anti-plane shear of a tunnel in an elastic half-space under surface loading: analytic algorithm and approximate explicit solution," *Zeitschrift f¨ur angewandte Mathematik und Physik*, vol. 73, no. 1, 42 pages, 2022.

[37] M. Dai, P. Schiavone, and C.-F. Gao, "Influence of surface effect of the edge of a half-plane on the stress concentration around a nearby nanosized hole of arbitrary shape," *Quarterly Journal of Mechanics & Applied Mathematics*, vol. 69, no. 3, pp. 215–229, 2016.

[38] M. H. Aghchai, P. Moarefvand, and H. S. Rad, "On analytic solutions of elastic net displacements around a circular tunnel," *Journal of Mining and Environment*, vol. 11, no. 2, pp. 419–432, 2020.

[39] M. Dai, P. Schiavone, and C.-F. Gao, "Surface tension-induced stress concentration around an elliptical hole in an anisotropic half-plane," *Mechanics Research Communications*, vol. 73, pp. 58–62, 2016.

[40] H. N. Wang, G. S. Zeng, and M. J. Jiang, "Analytical stress and displacement around non-circular tunnels in semi-infinite ground," *Applied Mathematical Modelling*, vol. 63, pp. 303–328, 2018.

[41] F. Pinto and A. J. Whittle, "Discussion of elastic solution for tunneling-induced ground movements in clays," *International Journal of Geomechanics*, vol. 6, no. 1, pp. 72-73, 2006.